Numerical Study of Energy-saving Mechanism of Duct on a VLCC with Real-geometry Propeller

Yuhai, Kong Weiping, Cai Rongquan，Wang Jinbao, Zhang Yuefeng
Marine Design and Research Institute of China(MARIC), Shanghai 200011, China

Abstract
Numerical self-propulsion simulation of a VLCC with real-geometry propeller was done on the basis of commercial software. The influence of energy-saving duct(ESD) on the propulsive performance was studied, and power prediction was carried out in the way ITTC recommended. CFD result agrees with model test. The mechanism of duct's influence on wake field, ship's resistance, and propulsive performance was researched and analyzed in detail. The influence of the symmetry of left and right duct was also investigated.Field information in this paper can be applied for duct's optimization design.
Key words: Real-geometry propeller, Self-propulsion numerical simulation, Duct, Energy-saving, Mechanism

1. Introduction

Recently, the energy problem is becoming more and more serious with industrial progress. Energy saving technologies are attracting much attention in the marine industry. The International Maritime Organization (IMO) is speeding up the process of developing Green-shipbuilding, and provides a series of energy indices, such as the EEDI. Against this background, a 30.8 DWT VLCC is used as the object and an energy saving device-stern duct is numerically simulated to study the influence of the duct on the wake field, the ship resistance and power of self-propulsion in this paper. Related articles to this paper refer to Reference 1, 2 and 3.

2.Mathematical modeling and Numerical Method

The right-handed global coordinate system (x,y,z) is defined as positive x in the ship moving direction ,positive y port, and positive z upward as show in Fig. 1.

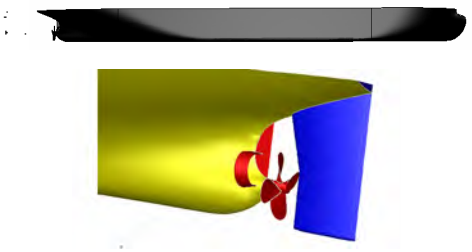

Fig. 1. Coordinate System and model sketch

The governing equations are written as follows.

$$\frac{\partial r}{\partial t}+\nabla\cdot(r\mathbf{v})=0 \qquad (1)$$

$$\frac{\partial(r\mathbf{v})}{\partial t}+\nabla\cdot(r\mathbf{vv})=-\nabla p+\nabla\cdot\bar{\bar{t}}+r g \qquad (2)$$

where $\mathbf{v}$ is the velocity vector in the Cartesian coordinate system, p the static pressure, and $\bar{\bar{t}}$ the stress tensor given by

$$\bar{\bar{t}}\equiv m[(\nabla\mathbf{v}+\nabla\mathbf{v}^T)-\frac{2}{3}\nabla\cdot\mathbf{v}I] \qquad (3)$$

where m is the molecular viscosity, I the unit tensor, and the second term on the right hand side the effect of volume deformation. The Reynolds averaged Navier-Stokes equations can be written in Cartesian tensor form as

$$\frac{\partial r}{\partial t}+\frac{\partial}{\partial x_i}(r\mathbf{v}_i)=0 \qquad (4)$$

$$\begin{aligned}&\frac{\partial}{\partial t}(r u_i)+\frac{\partial}{\partial x_j}(r u_i u_j)\\&=-\frac{\partial p}{\partial x_i}+\frac{\partial}{\partial x_j}[m(\frac{\partial u_i}{\partial x_j}+\frac{\partial u_j}{\partial x_i}-\frac{2}{3}d_{ij}\frac{\partial u_l}{\partial x_l})]\\&+\frac{\partial}{\partial x_j}(-r\overline{u'_i u'_j})\end{aligned} \qquad (5)$$

where d_{ij} is the Kronecker delta, $-r\overline{u'_i u'_j}$ and the Reynolds stresses. These Reynolds stresses must be modeled to close equation (5), i.e., for turbulence closure. The VOF method is employed to handle the free-surface wave flow around the ship. Based on the local volume fraction of the q-th fluid, a_q, the appropriate variables and properties are assigned to each cell within the domain. The tracking of the interfaces between the phases is accomplished by the solution of a continuity equation for the volume fraction of phases. For the q-th phase, this equation has the following form.

$$\frac{\partial a_q}{\partial t}+\mathbf{v}\cdot\nabla a_q=0 \qquad (6)$$

$$\sum_{q=1}^{n} a_q = 1 \qquad (7)$$

$$r = \sum_{q=1}^{n} a_q r_q \qquad (8)$$

In the case of turbulence quantities, a single set of transport equations is solved, and the turbulence variables are shared by the phases throughout the field.

The computations were carried out using FLUENT v6.3. The governing equations were discretized using an implicit unsteady method. The second order accurate upwind scheme was selected for the convection terms, while the second order accurate central scheme was used for the diffusion terms and the volume fraction equation. The equations of the continuity and momentum were solved sequentially (Weiss and Smith, 1995). The Realizable k-ε turbulence model with non-equivalent wall functions was used for turbulence closure.

3. Numerical simulation

3.1 Computational model and condition

A very large crude carrier (VLCC) was selected for this case study. The main particulars are described in Table 1. For the Froude number of VLCC is 0.144, wave-making resistance is the small influence of the ship, so the double model is used in this paper.

Table 1 main particulars of VLCC

	Fullscale	modelscale
Lpp（m）	320	6.4
B（m）	60	1.2
T（m）	20.5	0.41
Cb	0.818	0.818
S（m^2）	27930.7	5.586
V	15.7kn	1.142m/s
D（m）	10	0.2
λ	50	

3.2 The installation of the ESD

The dimension of ESD is show in Fig. 2, and the installation of the ESD is show in Fig. 3. For symmetrical allocation of left and right ESDs α=4°, β=4°, γ=2° is used on both sides. While for asymmetrical allocation α=4°, β=4°, γ=2° is used on the left side and α=2°, β=2°, γ=1° on the right side. Commutate-board connect the double ESDs.

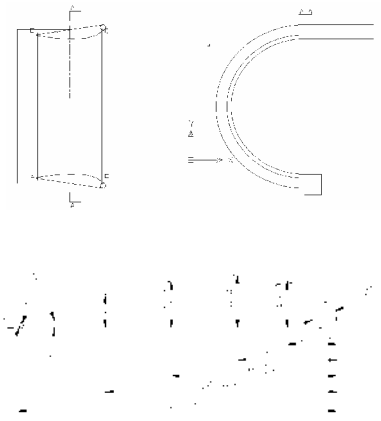

Fig. 2. ESD's dimension

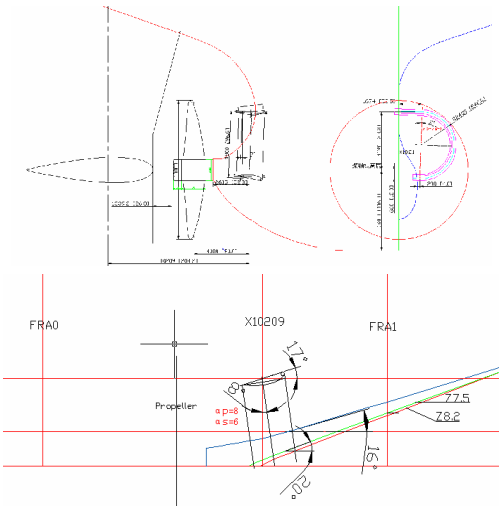

Fig. 3. Allocation of the ESD

3.3 Resistance and wake simulation

The resistance result is shown in Table 2

Table 2 resistance simulation

	Rt（N）	Increasement ratio
No ESD	30.605	/
Symmetrical ESD	30.48	0.4%
ASymmetrical ESD	30.62	0.06%

From the table we can see, the resistance of ESD is less than 0.4% Rt, one reason is that the surface area of the ESD and the projected area in x direction is small.

The wake results are shown in Fig. 4~ Fig. 6. Fig. 4.is Axial wake contour at propeller disc, Fig. 5 is velocity vector, and Fig.6 is axial wake along the circumferencial angle at different radii.

(Set 12 clock as 0°and increase anti-clockwisely in this paper.)

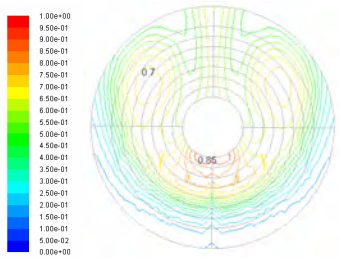

No ESD

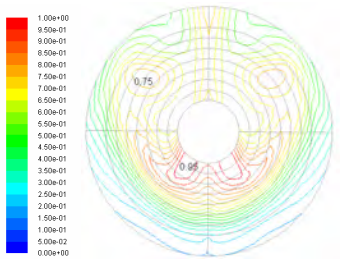

Symmetrical ESD

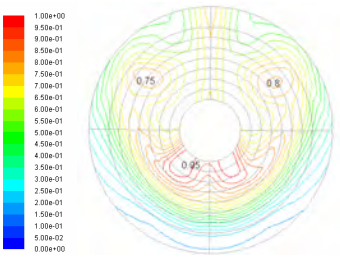

Asymmetrical ESD

Fig. 4. Axial wake contour at propeller disc

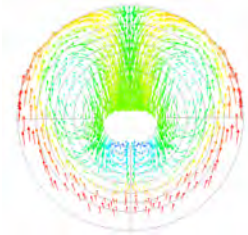

No ESD

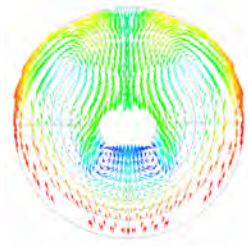

Symmetrical ESD

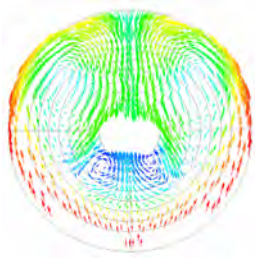

Asymmetrical ESD

Fig. 5. Velocity vector at propeller disc

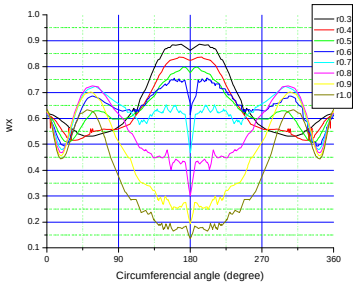

No ESD

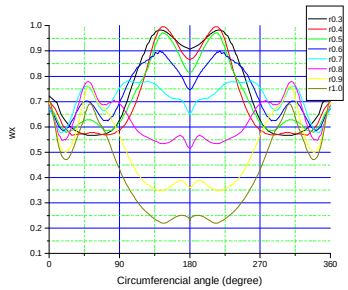

Symmetrical ESD

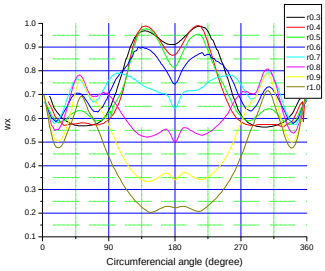

Asymmetrical ESD

Fig.6. Axial wake along the circumferencial angle at different radii at propeller disc

From Fig.4~6,we can see the wake velocities are increased with ESD. In the area 0°~90° and 270°~360°, the maximum value of wake increases from 0.7 up to 0.75 and 0.8, while in the area of 90°~270°, the maximum value of wake increases from 0.85 up to 0.95. The wake average also increases of every radii.

The duct doesn't improve the uniformity of the wake at different radii, but it reduces the velocity difference

between the upper half part and the lower half part at the propeller disc plane.

For symmetrical ESD and asymmetrical ESD,the wake and vector is identical on the left propeller plane. We can see that the ducts on both sides of ship don't interfere with each other on the flow around the ship.

Quantitative comparison of wake change with and without ESD is presented in table3.

Table 3 The average value of axial wake at propeller plane at different radii and area

	r0.3	r0.4	r0.5	r0.6	r0.7	r0.8	r0.9	r1.0
No	0.662	0.633	0.635	0.642	0.603	0.533	0.442	0.359
Sym	0.779	0.742	0.736	0.740	0.731	0.622	0.523	0.461
Asym	0.781	0.749	0.745	0.743	0.731	0.623	0.522	0.462

0° ~90°	90° ~180°	180° ~270°	270° ~360°	0° ~360°
0.552	0.402	0.402	0.552	0.477
0.594	0.487	0.487	0.594	0.541
0.597	0.484	0.481	0.604	0.542

To get more information from ESD, let's set the plane x=0.19m as the characteristic plane A which is near the outlet of the duct, we can see the influence of the duct in this plane.

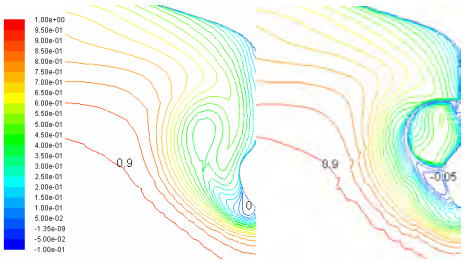

No ESD with ESD

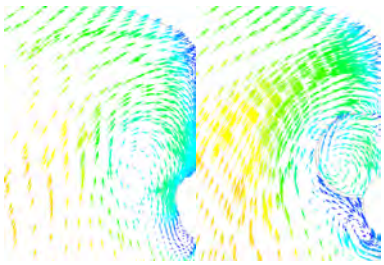

No ESD with ESD

Fig.7. The axial velocity (Vx/V0) and vector in characteristic plane A

From Fig.7 we can see the duct has restricted the eddy inside the duct, the eddy region becomes smaller and the strength becomes weaker. However obvious interference of lower part of duct on bilge eddy appears. The separation region becomes wider and the separation intensity also becomes stronger with ESD. Fig.8 provides more information..

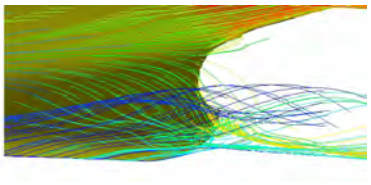

The streamlines of ship(No ESD)

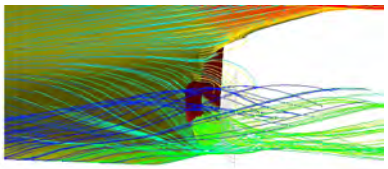

The streamlines of ship(Left ESD)

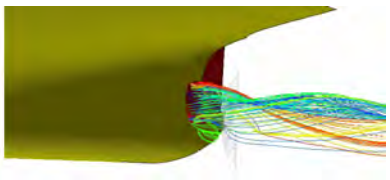

The streamlines of duct(Left ESD)

Fig.8. Comparison of streamlines

From Fig.8 we can see, the streamlines on the hull are blocked by the lower part of duct, making separation appear at back-and-downward region of the duct, which does not exist without duct. It also explains the obvious increase of the numerical value of wake in the inner radii's region 90°~270° in Fig.4.

The streamlines from duct only pass through the region 0°~90° of the propeller plane; in other words, the region 90°~180° on the propeller plane are not directly influenced by streamlines from duct. From ahead we see, the duct causes separation at its lower part. The inner radii on region 90°~180° on the propeller plane is downstream of the separation regoin below the duct. The wake at corresponding position changes obviously on the propeller plane because of the separation at upstream. This is the indirect influence caused by the duct.

In summary, the resistance variation induced by duct is very small, resistance is only a minor factor to the influence of ESD on propulsive performance; the axial wake in the propeller plane increased with duct, the duct causes obvious disturbance to the flow at the afterbody of the hull, it is main factor on the influence of ESD on propulsive performance.

3.4 Self-propulsion numerical simulation

To better understand the mechanism of ESD, numerical self-propulsion simulation with real-geometry propeller is performed. In this paper only two cases are treated: Ship without ESD and ship fitted with an asymmetrical ESD.

3.4.1 Open water test

The propeller for self-propulsion simulation is a right-rotation propeller designed by MARIC for 30.8w DWT VLCC, the particulars of the propeller are shown in Table 4.

Table 4 particulars of propeller

D (m)	0.2
$P_{0.7}/D$	0.667
Ae/Ao	0.54
Blade number	4
Rotation	right

Computational results of open water are compared with the test (MARIC) are shown in Fig.9. Numerical open water simulation refers to Reference 3.

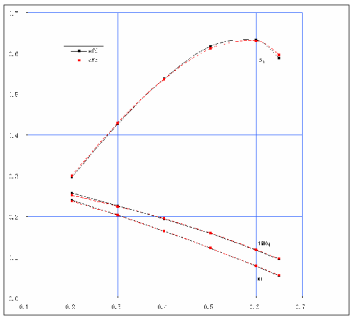

Fig.9. Open water performance curve of propeller

Computational results of open water agrees well compared with the test ones, between J=0.3 to J=0.6, the deviations of T、Q、η are smaller than 1%.

3.4.2 Numerical self-propulsion simulation of a VLCC with real-geometry propeller and power prediction

The results of numerical self-propulsion simulation of a VLCC with real-geometry propeller is shown in Table 5.

Table 5 data at self-propulsion point

	N(rps)	T（N）	Q（N •m）
No ESD	8.54	19.77	0.5005
With ESD	8.30	19.06	0.4784

The results of power prediction was carried out in the way ITTC recommended shown as in Table 6.

Table 6 Power prediction results

	No ESD	ESD
Js	0.4225	0.4278
Kq0s	0.1805	0.1786
η0s	0.5781	0.5831
ηH	1.1690	1.2090
Ns	1.2552	1.2408
ηds	0.6258	0.6549
Pds	24793.1	23643.7
ESR	4.6%	

The ESR of CFD contrast ESD to No ESD' Pds is 4.6%，which is appreciably bigger than EFD(MARIC) 3%.

Table 7 EFD of MARIC

Vs（kn）	ESR（%）
15	2.9
16	3.1

3.4.3 Analysis the influence of duct on propeller

In this paper, comparison is made with and without ESD at n=8.3556rps, the propeller at the same phase position relative to the hull. The plane 0.1d in front of the propeller disc is chosen as characteristic plane B, and the plane 0.1d after the plane at propeller as characteristic plane C. Axial wake at plane B and C as shown in Fig11-12.

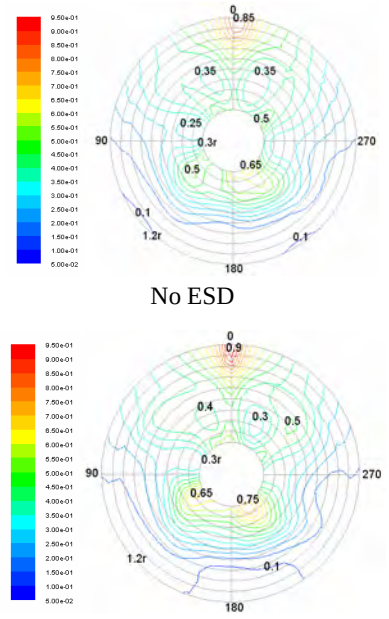

Fig.10. Axial wake contour at characteristic plane B

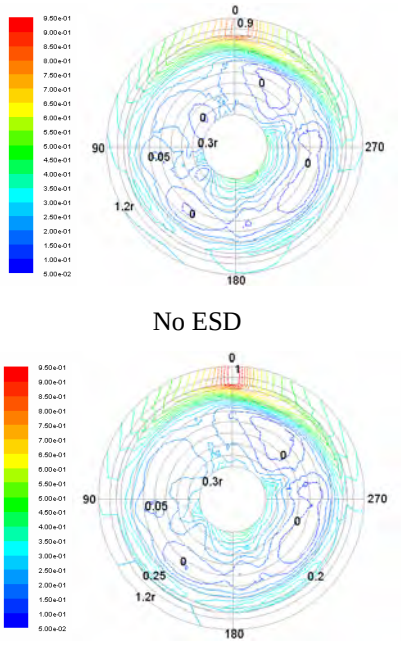

Fig.11. Axial wake contour at characteristic plane C

To Compare the ESD with No ESD case, it is clear that:

(1) The axail wake increased on the plane B.

(2) The axail wake is almost identical on plane C.

The surface-average value of axial wake is listed in table 8. The surface-average value of axial wake in plane B is

bigger with ESD; while in plane C, the surface-average value of axial wake is almost the same.

Table 8 Surface-average value of axial wake in the area of 0.3≤r/R≤1.0

wx	characteristic plane B	characteristic plane C
No ESD	0.309	0.132
ESD	0.327	0.134

The vector on the characteristic plane is show Fig.12-13

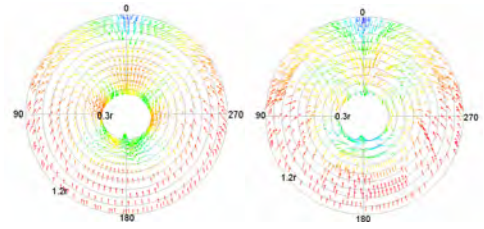

No ESD ESD

Fig.12. Vector at characteristic plane B

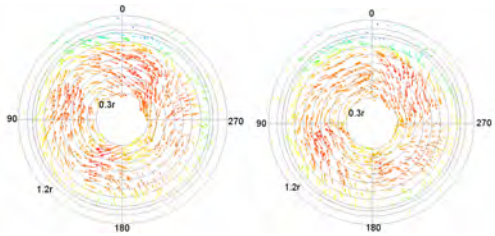

No ESD ESD

Fig.13. Vector at characteristic plane C

From Fig13 , we can see,

(1) There are obvious differences in the presence of vector in plane B.

(2) There are little difference in the presence of vector in plane C.

Tangential velocity at characteristic plane as shown in Fig.14-15

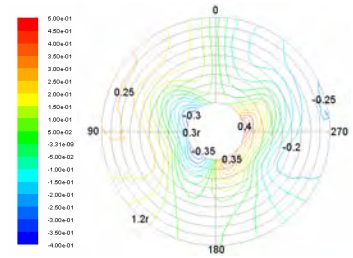

No ESD

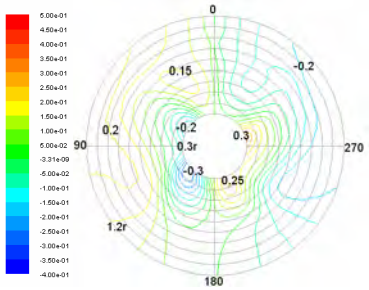

ESD

Fig.14. Tangential velocity at characteristic plane B

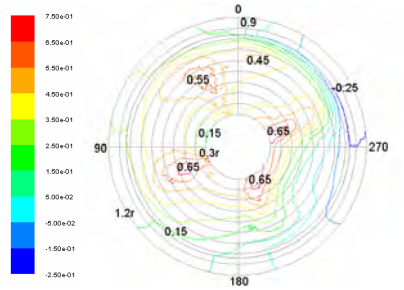

No ESD

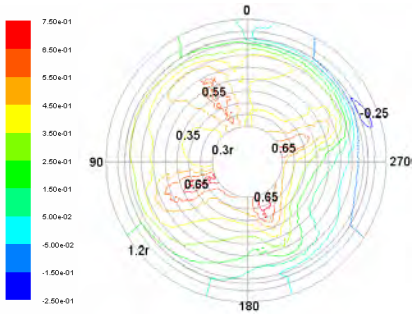

ESD

Fig.15. Tangential velocity at characteristic plane C

From Fig14-15 , we can see,

(1) The right-rotation tangential velocity is decreased, which produces favorable pre-rotation on plane B. There are little difference in the tangential velocity on plane C.

(2) The ESD reduces the difference of tangential velocity in the left side and right side before propeller; there is no difference in the plane after propeller.

Table 9 gives the detailed value.

Table 9 Surface-average value of tangential velocity in the area of 0.3≤r/R≤1.0

Vt/V	characteristic plane B	characteristic plane C
No ESD	0.0157	0.304
ESD	-0.0011	0.297

For right-rotation propeller, the tangential velocity value negative before the propeller is helpful for propulsive performance. So the ESD will be beneficial to enhance propulsive performance.

The pressure on the characteristic plane is shown Fig.16-17.

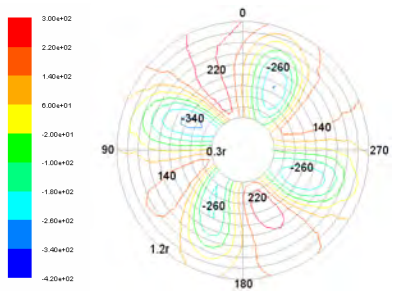

No ESD

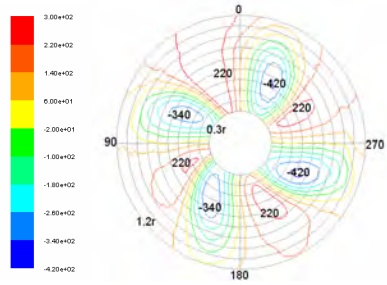

ESD

Fig.16. Pressure on characteristic plane B

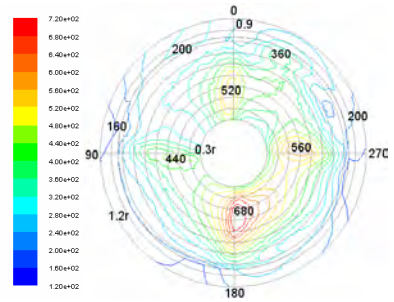

No ESD

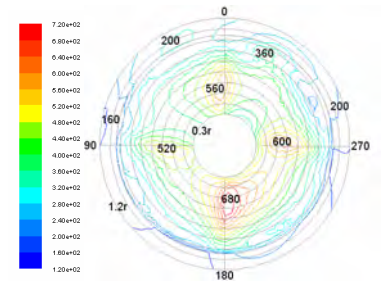

ESD

Fig.17. Pressure on characteristic plane C

The ESD make the negative pressure lower before propeller, and the positive pressure higher after propeller. The increase of pressure difference between B and C is beneficial for propulsive performance.

The surface-average of pressure is shown in table 10.

Table 10 Surface-average value of pressure in the area of $0.3 \leqslant r/R \leqslant 1.0$

P（pa）	characteristic plane B	characteristic plane C	C-B
No ESD	-3.73	365.1	368.83
ESD	-20.43	386.7	407.13
Difference	-16.7	21.6	38.3

Obviously, the pressure difference C-B is increased with ESD.

3.4.4 The influence of duct on hull

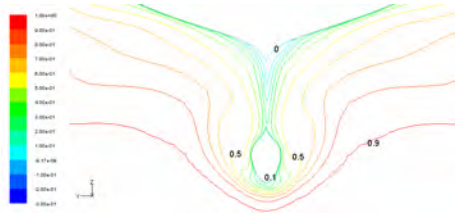

No ESD

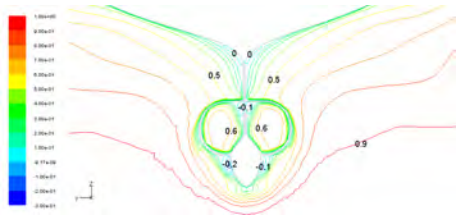

ESD

Fig.18 Axail velocity（Vx/V0）on characteristic plane A

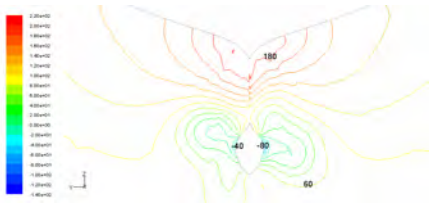

No ESD

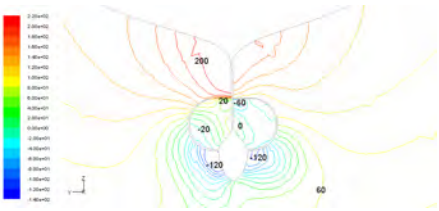

ESD

Fig.19 Pressure contour on characteristic plane A

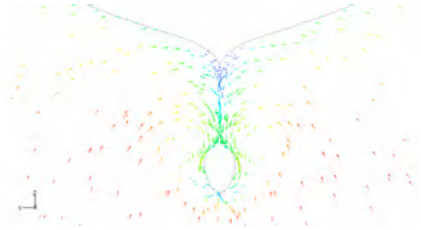

No ESD

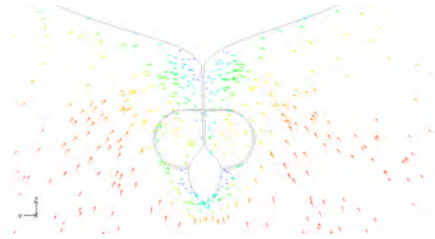

ESD

Fig.20 Vector at characteristic plane A

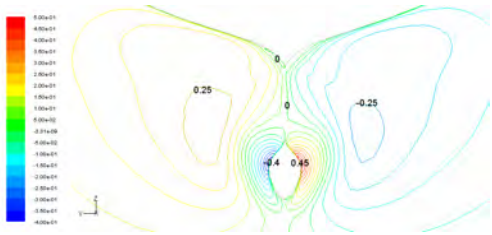

No ESD

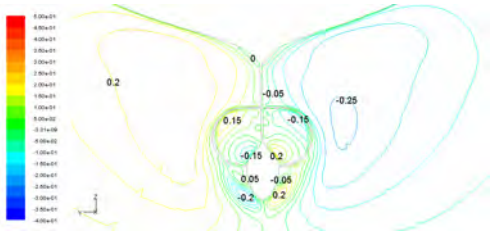

ESD

Fig.21 Tangential velocity contour on plane A

From Fig.18-21 we can see, the operating propeller make the flow field on the afterbody of the hull asymmetrical, and the duct attenuates the asymmetry of the local flow. The duct reduce the pressure difference between two sides. The suction of operating propeller doesn't improve the separation on the hull（refer to Fig 7）. On the contrary, the separation below the duct is strengthened by propeller rotation.

4. CONCLUSION

（1) The resistance variation induced by duct is very small.

（2) The axial wake velocity in the propeller plane is increased by the duct.

（3) The ESD produces a tangential velocity field which is beneficial for propulsive performance.

（4) The increase of pressure D-value between regions through the propeller is also beneficial for propulsive performance.

(5) The duct reduce the pressure difference between two sides.

(6) The suction of propeller doesn't improve the separation on afterbody of the hull. On the contrary,, the separation below the duct is strengthened by propeller rotation.

5. REFERENCE

1 Jie Dang, (2011) An Exploratory Study on the Working Principles of Energy Saving Devices(ESDs), Symposium on Green Ship Technology(Geenship'2011), Wuxi, China.

2 Jie Dang, (2012) An Exploratory Study on the Working Principles of Energy Saving Devices(ESDs)-PIV,CFD Investigations and ESD Design Guidelines, Proceeding of the 31st International Conference On Ocean, Offshore and Arctic Engineering(OMAE2012), Rio de Janeiro, Brazil.

3 Kong Weiping, (2012) Numerical Study on the Energy-Saving Rate of Stern Duct, [M],China. (in Chinese)